Molecular Size Effect on the Site Dependent Photofragmentation of N and O K-Shell Excited $CH_3CO(CH_2)_nCN$ ($n = 0-3$)

K. Okada, S. Tanimoto, T. Morita, and K. Saito

Department of Chemistry, Hiroshima University, Higashi-Hiroshima 739-8526, Japan

T. Ibuki*

Kyoto University of Education, Fushimi-ku, Kyoto 612-8522, Japan

T. Gejo

Institute for Molecular Science, Okazaki 444-8585, Japan

Received: February 10, 2003; In Final Form: July 24, 2003

Molecular size effects on the site specific photofragmentation of a core excited molecule were investigated by exciting the N and O K-shells for a series of $CH_3CO(CH_2)_nCN$ ($n = 0-3$) in which the O and N atoms were separated by successively inserting a CH_2 group between the two atoms. The photofragment ions coincident with total photoelectrons were observed by means of a reflectron type time-of-flight mass spectrometer. Little difference was observed in the fragmentation patterns between the N and O K-edges in exciting CH_3COCN, CH_3COCH_2CN, and $CH_3CO(CH_2)_2CN$. Clear discrimination was observed in the long chained $CH_3CO(CH_2)_3CN$.

1. Introduction

Photoexcitation of the K-shell electron creates a core hole in a molecule. Direct ionization of the innermost 1s electron in the molecule composed of light atoms such as C, N, and O usually leads to double electron ejection via normal Auger decay. The mode of excitation of a core electron to a vacant molecular orbital (MO) is called the resonance Auger process: One electron in a valence MO drops down to fill the core hole, and the electron initially excited to the vacant MO is released as an Auger electron. Thus, the molecules are populated in different electronic states of +1 charged ions. This mode is called the participant resonance Auger process. On the other hand, if the core electron initially excited to the vacant MO does not take part in the decay, one electron in the valence MO fills the core hole and another valence electron is released as an Auger electron, the final states of which are referred to as two-hole one-particle states. This mode of excitation is called spectator resonance Auger decay. In general, the lifetimes of core hole molecules followed by Auger decays are of the order 10^{-15} s, being shorter than the periods of molecular vibration and rotation ($\approx 10^{-13}$ s), and hence nonstatistical chemical reactions are expected. It has been of great interest to observe the products formed by the excitation of the innermost 1s electron of a specific atom in a molecule. Such evidences for atom-selective soft X-ray chemistry of gaseous molecules have been studied for N_2O,[1,2] O_3,[3] CF_2CH_2,[4] CF_3CH_3,[4,5] chlorofluorocarbons,[6−8] $(CH_3)_2CO$,[1] $Pb(CH_3)_4$,[9] *n*- and 2-propanol,[10] and other organic molecules,[11,12] by exciting K-edges. These works have been performed with the expectation that a chemical bond scission can occur in a limited area around the atomic site of excitation; that is, a site specific reaction following normal and/or resonance Auger decay is to be expected.

In a recent paper we reported that photofragmentation of the C and N K-shell excited CF_3CN competes with the intramolecular energy relaxation of the CF_3 group.[13] Fragmentation patterns were little dependent on the electronically excited states of CF_3CN. We anticipate that the effective area of site specific fragmentation of a core excited molecule would be estimated by changing the length of a molecule. In this work the molecular size effect was investigated by successively inserting a CH_2 group between the CO and CN functional groups in a series of $CH_3CO(CH_2)_nCN$ and then selectively exciting the O and N K-shells.

2. Experiment

Synchrotron radiation (SR) from UVSOR at the Institute for Molecular Science (IMS) was dispersed using a constant-deviation constant-length spherical grating monochromator, in which three gratings with different grooves were installed to obtain 30−700 eV photons.[14] An Al thin filter was used in order to reduce the scattered stray light. The dispersed soft X-ray flux was monitored by a silicon photodiode and recorded simultaneously as the photocurrent. All spectra were normalized by the photocurrent in order to correct for fluctuations in the dispersed photon flux.

A reflectron type time-of-flight (R-TOF) mass spectrometer was mounted at the magic angle with respect to the linearly polarized electric vector of the SR beam.[15] The sample was introduced into the chamber as an effusive jet. The R-TOF mass spectrometer was designed to collect fragment ions with kinetic energies up to $\cong$10 eV at $m/e = 70$: A high electrostatic field (−1.5 kV/cm) was applied for extracting fragment ions, and two lens systems were installed to focus the ions on a microsphere plate detector. An energy resolution about 1 eV of the primary SR was employed for the acquisition of R-TOF mass spectra because of the weak SR intensity.

* Corresponding author. Telephone: +81-75-644-8276. Fax: +81-75-645-1734. E-mail: ibuki@kyokyo-u.ac.jp.

10.1021/jp030172t CCC: $25.00
Published on Web 09/19/2003

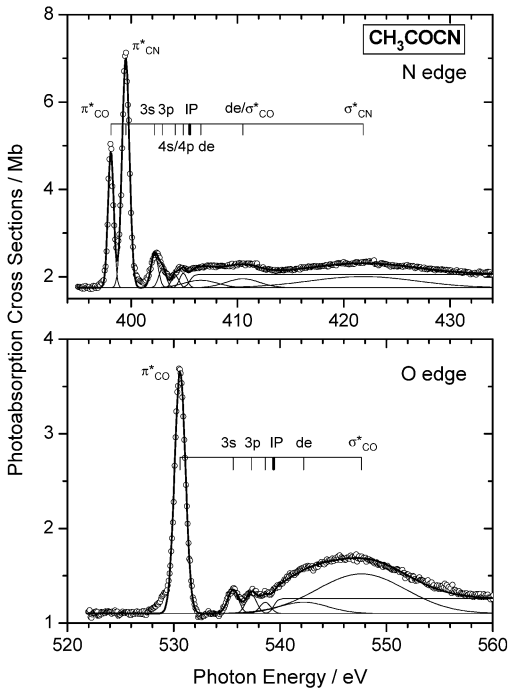

Figure 1. Total photoabsorption cross sections of CH_3COCN in the N and O K-edges. The open circles are the experimental data. The solid curves are obtained by a least-squares curve fitting. The peak assignments given in Table 1 and the estimated ionization potentials are shown. The "de" means double excitation.

The total cross section of photoabsorption was obtained by using a Samson type double ion chamber[16] with an Al thin filter at the front and the silicon photodiode at the end, with the distance being 23 cm. This chamber was attached to the end of the main chamber. The peak height of the photoabsorption band is influenced by the energy resolution of the primary SR beam $E/\Delta E$, which has been reported to be better than 2000 around 400 eV for measuring the photoabsorption spectrum under the present experimental conditions.[14] Uncertainty in the total cross section of photoabsorption was estimated to be less than 10%.

Commercial samples of CH_3COCN and $CH_3CO(CH_2)_3CN$ with a stated purity better than 95% were supplied by Sigma-Aldrich Japan Co. Ltd. and used after distillation in a vacuum to collect the middle fraction. The samples of CH_3COCH_2CN and $CH_3COCH_2CH_2CN$ were synthesized according to the procedures published in the previous papers by Claisen[17] and Kawasaki et al., respectively.[18] The ^1H NMR spectrum was recorded at 400 MHz in $CDCl_3$ with TMS as an internal reference: δ values in $CDCl_3$ were 3.18 (s, 3H) and 4.70 (s, 2H) for CH_3COCH_2CN and 2.21 (s, 3H), 2.57 (t, $J = 6.8$ Hz, 2H), and 2.83 (t, $J = 6.8$ Hz, 2H) for $CH_3CO(CH_2)_2CN$. These synthesized samples were also distilled in a vacuum before use.

3. Results and Discussion

3.1. Total Photoabsorption Cross Sections in the N(1s) and O(1s) Regions. *3.1.1. CH_3COCN.* Photoabsorption spectra of CH_3COCN at the N- and O-edges have some structures as shown in Figure 1: Two π^* molecular orbitals (MO's) are spread over the molecule, and then we assign the distinguishable peaks at 398.1 and 399.5 eV to the $\pi^*_{CO} \leftarrow$ N(1s) and $\pi^*_{CN} \leftarrow$ N(1s) resonant transitions, respectively. In the energy region higher than 401 eV some electronically excited states are overlapped and/or embedded. To estimate their peak positions, we carried out a least-squares peak fitting by using Gaussian functions, and the results are shown in Figure 1. The ionization potential (IP) of N(1s) in CH_3COCN has not been reported, so far as we know. The IP is estimated to be 405.5 eV in analogy with the $N(1s)^{-1}$ of $CH_2{=}CHCN$ and CH_3CN.[19] The peaks at 402.2, 402.9, and 404.1 eV exposed by the peak fitting have the quantum defects $\delta = 1.0$, 0.7, and 0.8, respectively, and they are assigned to the 3s, 3p, and 4s/4p Rydberg levels. The band at 404.9 eV is overlapped by some high Rydberg transitions. The broad band peaked at 421.8 eV is assigned to the $\sigma^*_{CN} \leftarrow$ N(1s) excitation. The humps peaked at 406.5 and 410.5 eV are tentatively assigned to the double excitation, as was observed in the N K-shell spectrum of CH_3CN.[20] The latter peak at 410.5 eV is probably overlapped by the σ^*_{CO} excitation. These assignments are summarized in Table 1.

TABLE 1: Energy, Term Value, Quantum Defect, and Proposed Assignments for CH_3COCN in the N and O K-Shell Regions

energy (eV)	term value (eV)	quantum defect δ	proposed assignment
	N K-Shell Excitation		
398.1	7.4		π^*_{CO}
399.5	6.0		π^*_{CN}
402.2	3.3	0.97	3s
402.9	2.6	0.71	3p
404.1	1.4	0.81	4s/4p
404.9	0.6		high Rydberg
(405.5)[a]			IP
406.5	−1.0		double excitation
410.5	−5.0		σ^*_{CO}/double excitation
421.8	−16.3		σ^*_{CN}
	O K-Shell Excitation		
530.6	8.5		π^*_{CO}
535.6	3.5	1.0	3s
537.3	1.8	0.3	3p
538.6	0.5		high Rydberg
(539.1)[a]			IP
542.2	−3.1		double excitation
547.7	−8.6		σ^*_{CO}

[a] Estimated value from ref 19.

The bottom panel in Figure 1 shows the peaks observed in the O K-shell excitation. The distinct peak at 530.6 eV is assigned to the $\sigma^*_{CO} \leftarrow$ O(1s) transition. The 3s and 3p Rydberg levels are deduced by using the estimated IP of 539.1 eV for the $O(1s)^{-1}$ of C_2H_5OCOCN.[19] The peak assignments are given in Table 1.

3.1.2. General Photoabsorption Features of $CH_3CO(CH_2)_nCN$ ($n = 1-3$). The general features of the total photoabsorption cross sections of $CH_3CO(CH_2)_nCN$ ($n = 1-3$) in the N and O K-shell regions are shown in Figures 2 and 3, respectively, together with the results for CH_3COCN. The strong peaks around 400 and 530.5 eV are assigned to the $\pi^*_{CN} \leftarrow$ N(1s) and $\pi^*_{CO} \leftarrow$ O(1s) transitions, respectively. The weak and broad bands around 420 eV in Figure 2 are the $\sigma^*_{CN} \leftarrow$ N(1s) excitations, and those around 545 eV in Figure 3 are the $\sigma^*_{CO} \leftarrow$ O(1s) transitions. The peak positions of Rydberg transitions and double excitation become vague as the molecular size gets larger.

3.2. Site Specific Photofragmentation. Figures 4 and 5 show the typical fragmentation patterns of R-TOF mass spectra of CH_3COCN and $CH_3CO(CH_2)_2CN$, respectively, in which the N(1s) and O(1s) electrons are ionized and excited into the π^* levels. The peak intensities are expressed by normalizing with the maximum peak observed at the $O(1s)^{-1}$ ionization, that is, $m/e = 12$ in CH_3COCN and $m/e = 15$ in $CH_3CO(CH_2)_2CN$. The contribution of valence electrons was subtracted by measuring R-TOF mass spectra at photon energies just below the K-edges. The H^+ fragment ion was observed, but we are

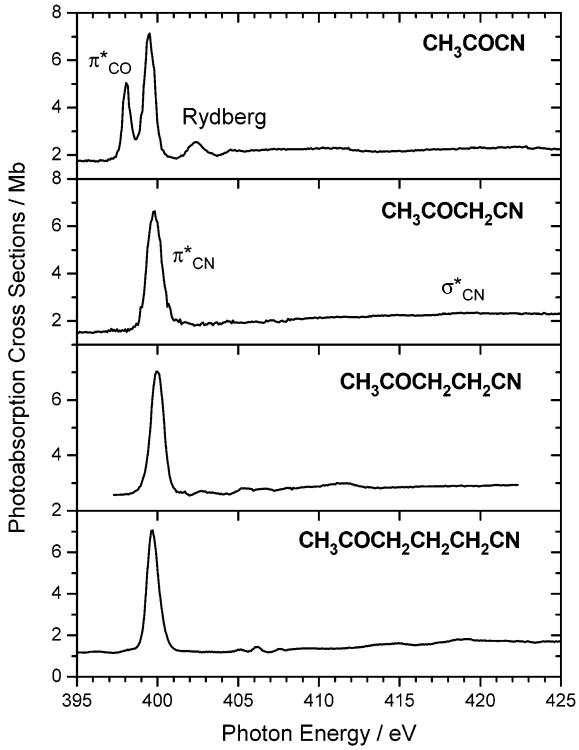

Figure 2. Total photoabsorption cross sections of $CH_3CO(CH_2)_nCN$ ($n = 0-3$) in the N K-shell regions.

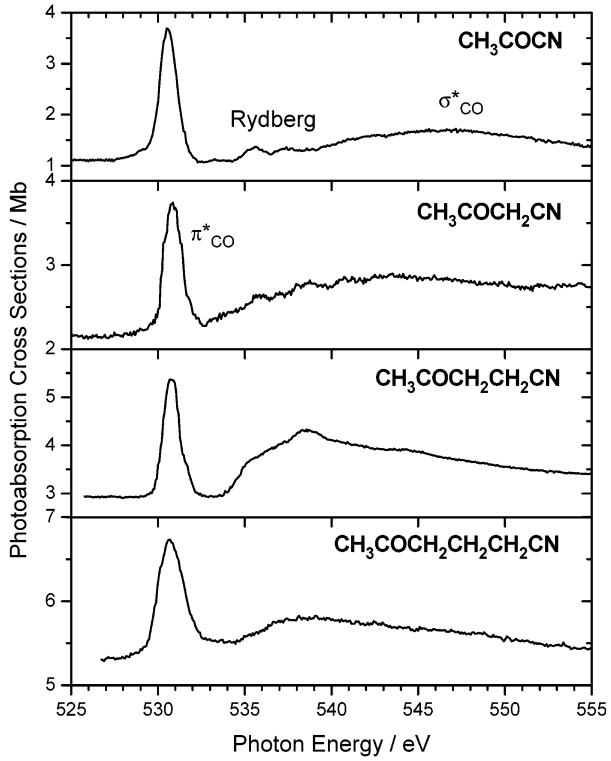

Figure 3. Total photoabsorption cross sections of $CH_3CO(CH_2)_nCN$ ($n = 0-3$) in the O K-shell regions.

afraid that the H^+ ion is not completely collected, since it is ejected into various directions with high velocity. Thus, the H^+ peak is not shown in the figures. The fragment ion exceeding $m/e = 60$ was not observed or was negligibly small. The fragmentation patterns of CH_3COCH_2CN (not shown) were similar to those of $CH_3CO(CH_2)_2CN$ in Figure 5.

Some features in Figures 4 and 5 are summarized in the following: The major fragment ions generated in the N and O

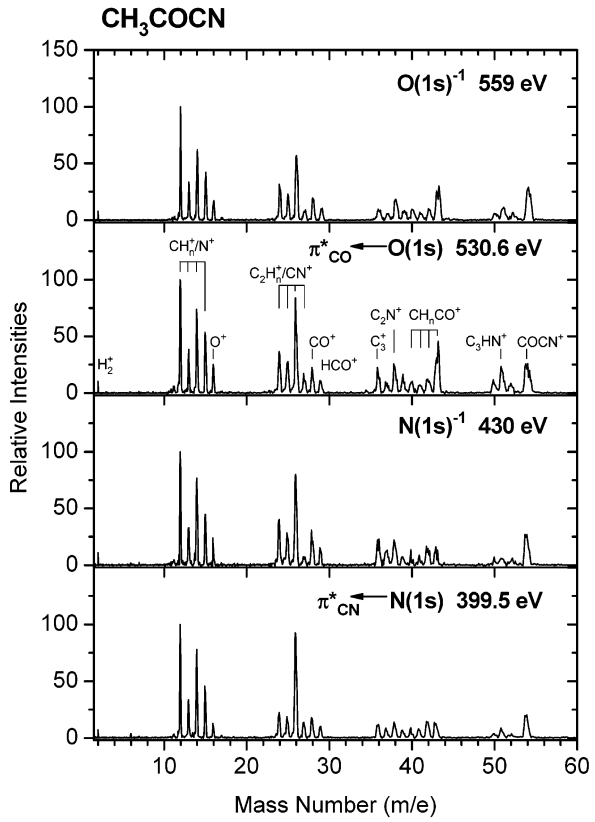

Figure 4. Reflectron type time-of-flight mass spectra of CH_3COCN excited at the O and N K-edges. The number of hydrogen atoms is $n = 0-3$ for CH_n^+, $C_2H_n^+$, and CH_nCO^+.

K-shell excitation of CH_3COCN are C^+, CH_2^+ or N^+, CN^+, CH_3CO^+, and $COCN^+$. We think that the mass at $m/e = 26$ is overwhelmingly composed of CN^+ though a small amount of $C_2H_2^+$ may be in existence. The yield of CN^+ fragment ion at the N K-shell excitation is about 1.4 times as much as that at the O K-shell. By contrast, the yield of CH_3CO^+ at the O K-edge is 2.7 times as much as that at the N K-shell excitation. The K-shell excitation of $CH_3CO(CH_2)_2CN$ shown in Figure 5 mainly produces the fragment ions of CH_3^+, CH_2^+ or N^+, $C_2H_2^+$ or CN^+, $C_2H_3^+$, $CHCN^+$, and CH_nCO^+ ($n = 2, 3$). The fragment ion at $m/e = 39$ is assignable to $CHCN^+$, and the disappearance of $COCN^+$ at $m/e = 54$ observed in CH_3COCN is reasonable. The yields of ($CH_2^+ + N^+$) and ($C_2H_2^+ + CN^+$) at the N K-shell excitation are, respectively, 2.0 and 1.7 times as much as those at the O K-edge, being due to the selective ionization of the $(CH_2)_2CN$ group at the N(1s) excitation. The prominent product at the O K-shell excitation is again CH_3CO^+, being 1.9 times as much as the yield at the N-edge. We do not think, however, that the differences observed in the N and O K-shell excited CH_3COCN and $CH_3CO(CH_2)_2CN$ are the clear site specific photofragmentation from the viewpoint of chemical reaction. In addition to this, the fragmentation patterns depending on the excited states such as the π^*, direct ionization, Rydberg, and σ^* (not shown) were nearly the same in the excitation of the N and O K-edges of $CH_3CO(CH_2)_nCN$ ($n = 0-2$).

Mass spectra of $CH_3CO(CH_2)_3CN$ excited at the N and O K-shells are shown in Figure 6 after correcting the contribution of valence electrons. It is clear that the formation of CH_3CO^+ at the O K-edge excitation overwhelms others and it reaches to 37% of the total products. The fragment ions at $m/e = 15$ (CH_3^+), 16 (O^+), and 41−43 (CH_nCO^+) undoubtedly originate in the CH_3CO group of $CH_3CO(CH_2)_3CN$. Thus, we denote the sum of them by "O-side products" in Table 2. Many kinds of

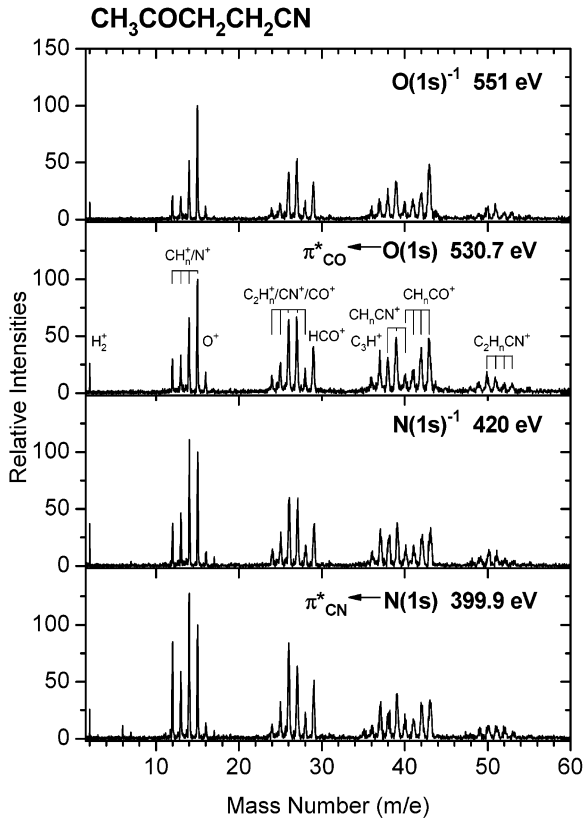

Figure 5. Reflectron type time-of-flight mass spectra of $CH_3CO(CH_2)_2CN$ excited at the O and N K-edges. The number of hydrogen atoms is $n = 0-3$ for CH_n^+, CH_nCO^+, and $C_2H_nCN^+$; $n = 0-4$ for $C_2H_n^+$; and $n = 0-2$ for CH_nCN^+.

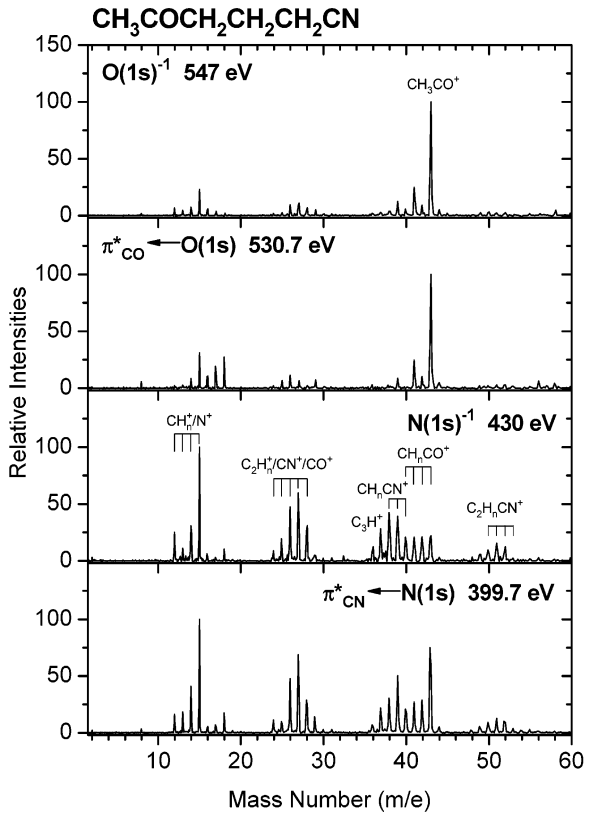

Figure 6. Reflectron type time-of-flight mass spectra of $CH_3CO(CH_2)_3CN$ excited at the O and N K-edges. The number of hydrogen atoms is $n = 0-3$ for CH_n^+, CH_nCO^+, and $C_2H_nCN^+$; $n = 0-4$ for $C_2H_n^+$; and $n = 0-2$ for CH_nCN^+.

small fragment ions are produced via the N K-shell excitation, in which the strongest one is CH_3^+, being 10% of the total fragment ions produced. The fragment ions in the $m/e = 24-27$, 38−39, and 50−53 regions are assignable to $C_2H_n^+$ ($n = 0-3$) and CN^+, CH_nCN^+ ($n = 0, 1$), and $C_2H_nCN^+$ ($n = 0-3$), respectively. They clearly originate in the $(CH_2)_3CN$ group of $CH_3CO(CH_2)_3CN$, and thus the sum of them is denoted by "N-side products". The yield of "O-side products" at the O K-shell excitation reaches 62% of the total fragment ions and decreases to 28% at the N K-shell excitation, while that of the "N-side products" shows the inverse tendency; that is, it increases from 17% at the O(1s) excitation to 40% at the N(1s) edge, as given in Table 2. These observations are in contrast to the results of $CH_3CO(CH_2)_2CN$ shown in Figure 5: The yields of the "O-side products" and "N-side products" of $CH_3CO(CH_2)_2CN$ do not show characteristic distributions. Miscellaneous fragment ions which are difficult to be assigned to the N-side or O-side products are increased by shortening one CH_2 segment.

After the K-shell excitation, the positive hole is occupied by a valence electron through Auger decay and then the hole moves to a valence MO to break a chemical bond. The configurations of some outer valence MO's representation in the ground states $CH_3CO(CH_2)_nCN$ ($n = 2, 3$) are expressed as the following where the core orbitals on C, N, and O are ignored in the numbering scheme:

$$n = 2: \quad ...(3a'')^2(4a'')^2(12a')^2(13a')^2(5a'')^2(14a')^2$$

$$n = 3: \quad ...(4a'')^2(5a'')^2(14a')^2(15a')^2(6a'')^2(16a')^2$$

The outermost 14a′ for $n = 2$ and 16a′ for $n = 3$ MO's are the σ-HOMOs localized on the CH_3CO group with the n_O, σ_{CC}, and σ_{CH} characters. The MO's from the second 5a″ and 6a″ to the fourth 12a′ and 14a′ orbitals are strongly localized on the $(CH_2)_nCN$ group. The inner 4a″ or 5a″ valence MO's are spread over the molecule. The characters of the valence MO's which fill the 1s hole and then release an Auger electron are closely similar between the two compounds. Thus, it is expected that the mass spectra of $CH_3CO(CH_2)_nCN$ after the Auger electron emission would be similar for $n = 2$ and 3. The fragmentation patterns observed are, however, different, as shown in Figures 5 and 6 for $n = 2$ and 3, respectively. From this observation we believe that the valence MO's have little relation with the site specific photofragmentation shown above.

The site dependent decomposition observed probably results from the intramolecular energy relaxation competing with bond dissociation. The yield of CH_3CO^+ at the O K-edge is superior to that at the N K-shell excitation for all of the compounds studied in this work. The O(1s) electron in a series of $CH_3CO(CH_2)_nCN$ ($n = 0-3$) is initially excited and then the OC−C bond is preferentially broken after Auger electron ejection. In

TABLE 2: Fragment Ions Grouped into the O- and N-Atom Sides at the O and N K-Shell Excited $CH_3CO(CH_2)_nCN$ ($n = 2, 3$) with Yields Given in Percent[a]

	$CH_3CO(CH_2)_3CN$		$CH_3CO(CH_2)_2CN$	
	O(1s)[d]	N(1s)[e]	O(1s)[d]	N(1s)[e]
O-side products[b]	62	28	30	23
N-side products[c]	17	40	39	32

[a] Mass discrimination effects were minimized by applying a high electrostatic field of −1.5 kV/cm for extracting fragment ions, by focusing the ions with two lens systems, and by measuring signal rates as low as possible. [b] The sum of fragment ions at $m/e = 15-16$ and 41−43. [c] The sum of fragment ions at $m/e = 24-27$, 38−39, and 50−53. [d] O K-shell excitation. [e] N K-shell excitation.

this process a part of the intramolecular excess energy would be distributed into the vibrational modes of the $(CH_2)_nCN$ ($n = 0-3$) group, just as discussed in CF_3CN.[13] The exclusive formation of CH_3CO^+ from the O K-shell excited $CH_3CO(CH_2)_3CN$ is understandable if the vibrational modes of the $(CH_2)_3CN$ group act as an effective energy reservoir for the excess energy flowing from the initially excited O atom. The number of vibrational modes of the $(CH_2)_nCN$ group with $n = 3$ should be critical to suppress fragmentation of the $(CH_2)_3CN$ group into small ions. This explanation is also useful for the understanding of the fragmentation patterns observed in the N K-shell excitation: In this case the $(CH_2)_3CN$ group acts as a barrier of energy flow from the initially excited N atom to CH_3CO and simultaneously decomposes into small fragment ions to produce the "N-side products" composed of $C_2H_n^+$, CN^+, CH_nCN^+, $C_2H_nCN^+$, and so forth. For the molecules of $CH_3CO(CH_2)_nCN$ ($n \leq 2$), the number of vibrational modes of $(CH_2)_nCN$ ($n \leq 2$) would be insufficient to keep the $(CH_2)_nCN$ group being an efficient energy reservoir. The $(CH_2)_nCN$ ($n \leq 2$) group decomposes into ionic fragments at both the N and O K-shell excitation, and then the site specific fragmentation becomes vague.

4. Concluding Remarks

Total photoabsorption cross sections of the N and O K-edges in a series of $CH_3CO(CH_2)_nCN$ ($n = 0-3$) were measured and the N and O K-shells were separately excited. The strong site dependent photofragmentation was observed in the N and O K-shell excited $CH_3CO(CH_2)_3CN$: The CH_3CO^+ is the dominant product with the yield of 37% at the O K-shell excitation. The yield of "O-side products" composed of CH_nCO^+ ($n = 1-3$), CH_3^+, and O^+ reaches up to 62% at the O K-shell excitation and decreases to 28% at the N K-edge. By contrast, the yield of "N-side products" containing $C_2H_n^+$ ($n = 0-3$), CN^+, CH_nCN^+ ($n = 0, 1$), and $C_2H_nCN^+$ ($n = 0-3$) increases from 17 to 40% by changing the excitation site from O K- to N K-edge. Site specific photofragmentation was weak in $CH_3CO(CH_2)_nCN$ ($n = 0-2$) though the CH_3CO^+ formation at the O K-shell excitation is superior to the yield at the N K-edge. The photofragmentation depending on the electronically excited states was weak for the four molecules studied. It is suggested that the K-shell excited photofragmentation would compete with the intramolecular energy relaxation in $CH_3CO(CH_2)_nCN$ ($n = 0-3$).

Acknowledgment. The authors thank the staff of UVSOR at IMS for their operating the electron storage ring. They are also grateful to Dr. M. Yamashita and Professor Y. Yamamoto at Hiroshima University for their help in the syntheses of the samples. This work was supported by the IMS joint program, a Grant-in-Aid on Research for the Future "Photoscience" (Grant No. JSPS-RFTF-98P01202) from Japan Society for the Promotion of Science, and a Grant-in-Aid for Scientific Research from the Ministry of Education, Science, Sports, Culture and Technology of Japan.

References and Notes

(1) Eberhardt, W.; Sham, T. K.; Carr, R.; Krummacher, S.; Strongin, M.; Weng, S. L.; Wesner, D. *Phys. Rev. Lett.* **1983**, *50*, 1038.
(2) Murakami, J.; Nelson, M. C.; Anderson, S. L.; Hanson, D. M. *J. Chem. Phys.* **1986**, *85*, 5755.
(3) Gejo, T.; Okada, K.; Ibuki, T.; Saito, N. *J. Phys. Chem.* **1999**, *103*, 4598.
(4) Habenicht, W.; Baiter, H.; Müller-Dethlefs, K.; Schlag, E. W. *J. Phys. Chem.* **1991**, *95*, 6774.
(5) Müller-Dethlefs, K.; Sander, M.; Chewter, L. A.; Schlag, E. W. *J. Phys. Chem.* **1984**, *88*, 6098.
(6) Suzuki, I. H.; Saito, N.; Bozek, J. D. *Bull. Chem. Soc. Jpn.* **1995**, *68*, 1119.
(7) Suzuki, I. H.; Saito, N. *Int. J. Mass Spectrom. Ion Proccesses* **1997**, *163*, 229.
(8) Suzuki, I. H.; Saito, N.; Bozek, J. D. *J. Electron Spectrosc. Relat. Phenom.* **1999**, *101−103*, 69.
(9) Nagaoka, S.; Koyano, I.; Ueda, K.; Shigemasa, E.; Sato, Y.; Yagishita, A.; Nagata, T.; Hayaishi, T. *Chem. Phys. Lett.* **1989**, *154*, 363.
(10) Thomas, M. K.; Hatherly, P. A.; Codling, K.; Stankiewicz, M.; Rius, J.; Karawajczyk, A.; Roper, M. *J. Phys. B: At. Mol. Opt. Phys.* **1998**, *31*, 3407.
(11) Ibuki, T.; Okada, K.; Gejo, T.; Saito, K. *J. Electron Spectrosc. Relat. Phenom.* **1999**, *101−103*, 149.
(12) Ibuki, T.; Okada, K.; Saito, K.; Gejo, T. *J. Electron Spectrosc. Relat. Phenom.* **2000**, *107*, 39.
(13) Ibuki, T.; Okada, K.; Tanimoto, S.; Saito, K.; Gejo, T. *J. Electron Spectrosc. Relat. Phenom.* **2002**, *123*, 323.
(14) Hiraya, A.; Nakamura, E.; Hasumoto, M.; Kinoshita, T.; Sakai, K.; Ishiguro, E.; Watanabe, M. *Rev. Sci. Instrum.* **1995**, *66*, 2104.
(15) Ibuki, T.; Okada, K.; Saito, K.; Gejo, T.; Saito, N.; Suzuki, I. H. *Nucl. Instrum. Methods Phys. Res., A* **2001**, *467−468*, 1505.
(16) Samson, J. A. R. *Techniques of Vacuum Ultraviolet Spectroscopy*; John Wiley & Sons: New York, 1967; p 263.
(17) Claisen, L. *Ber. Dtsch. Chem. Ges. (Berlin)* **1892**, *25*, 1776.
(18) Kawasaki, Y.; Fujii, A.; Nakano, Y.; Sakaguchi, S.; Ishii, Y. *J. Org. Chem.* **1999**, *64*, 4214.
(19) Jolly, W. L.; Bomben, K. D.; Eyermann, C. J. *At. Data Nucl. Data Tables* **1984**, *31*, 433.
(20) Hitchcock, A. P.; Tronc, M.; Modelli, A. *J. Phys. Chem.* **1989**, *93*, 3068.